Improved Performance of Perylene-Based Photovoltaic Cells Using Polyisocyanopeptide Arrays

Sam Foster,[†] Chris E. Finlayson,*[,†] Panagiotis E. Keivanidis,*[,†] Ya-Shih Huang,[†] Inchan Hwang,[†] Richard H. Friend,[†] Matthijs B. J. Otten,[‡] Li-Ping Lu,[‡] Erik Schwartz,[‡] Roeland J. M. Nolte,[‡] and Alan E. Rowan[‡]

Cavendish Laboratory, JJ Thomson Avenue, Cambridge CB3 0HE, U.K., and Institute for Molecules and Materials, Radboud University Nijmegen, Toernooiveld 1, 6525 ED Nijmegen, The Netherlands

Received August 29, 2008; Revised Manuscript Received December 8, 2008

ABSTRACT: Photovoltaic devices incorporating perylene-substituted polyisocyanide materials have been demonstrated, using blend systems with polythiophene- and polyfluorene-based conjugated polymers. Prototypical structures with nominal (1:1) blend weight ratios of the polyisocyanide with poly(3-hexylthiophene) (P3HT) and poly(9,9′-dioctylfluorene-*co*-bis(*N*,*N*′-(4-butylphenyl))-bis(*N*,*N*′-phenyl)-1,4-phenyldiamine) (PFB) readily showed an order of magnitude improvement in power conversion efficiency, as compared to analogous blend architectures using a perylene (PDI) monomer, whereas the performance of strongly phase-separated F8BT (poly(9,9-dioctylfluorene-*co*-benzothidiazole) blend devices showed no such improvement. We propose that the use of polyisocyanide chains as a molecular template offers a method by which the morphology and connectivity of photovoltaic blends can be modified and enhanced.

1. Introduction

Substituted polyisocyanopeptides[1−3] are a recently developed class of "supramolecular" materials, where chromophoric moieties may be arranged in an ordered helical array around a polymer template; this is reminiscent of many structures seen in biological systems.[4] In particular, a number of recent studies[5−7] have reported perylene-substituted polyisoscyanides (pery-PIC), consisting of perylene diimide (PDI) units, which self-stack in a regular fashion around a rigid helical polyisocyanopeptide (PIC) backbone, stabilized by hydrogen bonding between peptide units. The perylene units are arranged into chiral "helter-skelter" arrays, which do not form the kind of crystalline molecular aggregates often seen with perylene derivatives, but rather the units overlap continuously along the chain.[7] The resulting polymer is highly rigid, with persistence lengths of up to 76 nm.[1,5−7] The chemical structure and bonding structure of the pery-PIC material are shown in Figure 1a,b. PDI (Figure 1c), and derivatives, are already well-studied as n-type molecular semiconductors in organic photovoltaics.[8]

In this paper, we investigate the effect of the increased ordering of the PDI units around a rigid polymer chain by direct comparison of the performance of photovoltaic (PV) devices containing blends of well-studied conjugated polymers (Figure 1d) with either molecular perylene molecules (PDI monomer) or the polyisocyanide perylene polymers. The increased overlap of the perylene units when ordered along a well-defined polymer chain is expected to offer several advantages over the more randomized orientation of a blend containing individual perylene molecules. In addition to the highly efficient migrational energy transfer observed in the pery-PIC system,[7] it is also possible that the high degree of ordering and electronic orbital overlap along the rigid PIC backbone has an advantageous effect on properties such as the conductivity and carrier mobility, as recently investigated using thin-film transistor architectures.[9] Improved excitonic interactions may increase the exciton diffusion length, improving efficiency of charge separation before recombination, while improved carrier mobility would improve the efficiency of charge transport to the electrodes in a PV device.

Since the optimization of these processes is of general applicability to the performance of all organic PVs,[10] it is hoped that it will be possible to apply this strategy of using "molecular scaffold" architectures to arbitrary blend systems, improving their performance within devices. Furthermore, the simple issue of connectivity of the components, in terms of whether there is a continuous conduction route from charge separation sites to the electrodes, may also be of importance. Given these issues, the possible advantages offered by the presence of the PIC chain are manifold but potentially rather complex. Previous studies have actually shown the negative effect of perylene aggregation with enhanced order characteristics on energy transfer.[8] The tendency of the perylene monomers to stack in 1D aggregates resulted in perylene crystallization and consequently phase separation, giving a decreased photovoltaic performance due to the trapping of electrons in "unconnected" perylene domains.

In this study the performance parameters of PV devices containing blends of pery-PIC, with three other well-studied semiconducting polymers (P3HT, PFB, and F8BT), was investigated. For comparison, we also study comparable blends using the respective PDI analogue.[11] Two of the three PV blend systems (with p-type components P3HT and PFB) have shown maximum power conversion efficiencies with the ordered pery-PIC architecture increasing by at least 1 order of magnitude, as compared to the PDI analogues, while the third blend system (with notionally p-type component F8BT) shows no significant enhancement in performance.

2. Experimental Section

Perylene-substituted polyisocyanide material (pery-PIC) was synthesized at the University of Nijmegen, according to previously reported protocols.[5−7] The particular batch used in these experiments had a mean molecular weight of 9×10^5 g/mol, corresponding to an inferred mean chain length of ∼180 nm.

Regioregular poly(3-hexylthiophene) (P3HT) was purchased from Plextronics ("Plexcore HP", lot #05-10192). Poly(9,9′-dioctylfluorene-*co*-bis(*N*,*N*′-(4-butylphenyl))-bis(*N*,*N*′-phenyl)-1,4-phenyldiamine) (PFB) and poly(9,9-dioctylfluorene-*co*-benzothidiazole)

* Corresponding authors. E-mail: cef26@cam.ac.uk. E-mail: pekeivan@imperial.ac.uk
† Cavendish Laboratory.
‡ Radboud University.

10.1021/ma801959w CCC: $40.75
Published on Web 01/13/2009

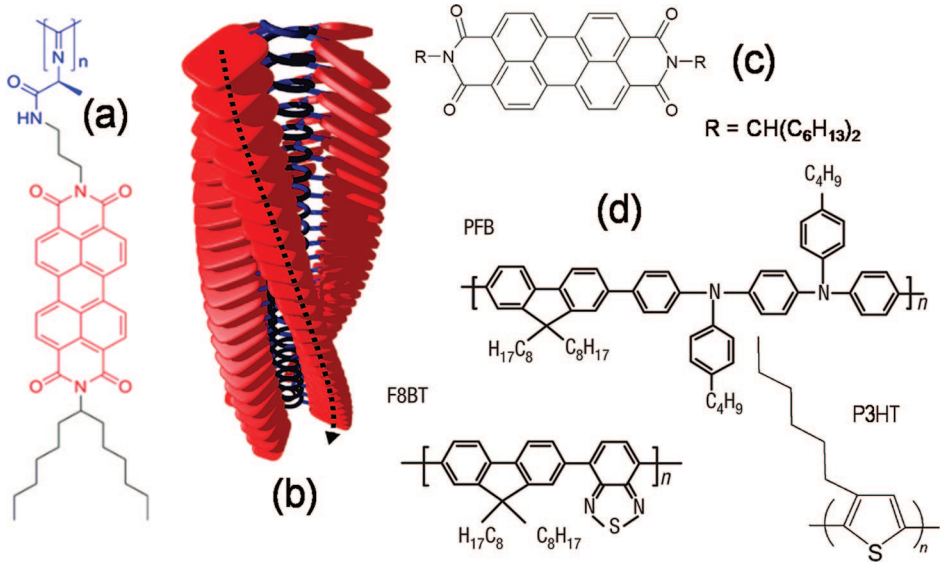

Figure 1. (a) Chemical structure of the perylene-substituted polyisocyanide material (pery-PIC) described in this paper, with a schematic representation of the resultant rigid, helical polymer shown in (b). (c) Shows the chemical structure of the perylene diimide (PDI) monomer used, while (d) gives the chemical structures of the conjugated polymers P3HT, PFB, and F8BT.

Table 1. Key Characteristics of the Thin-Film Blends Used in the Photovoltaic Devices Described in This Paper[a]

material/blend	thickness (nm) (by profilometry)	mean roughness (by AFM), nm	photoluminescence (PL) efficiency, %	PL quenching efficiency, %
pery-PIC only			8.2	
pery-PIC/F8BT	163.3 (±17.8)	±36.1	7.9	3.7
pery-PIC/PFB	176.8 (±11.1)	±27.3	6.0	26.8
pery-PIC/P3HT	171.5 (±4.6)	±13.6	1.3	84.1
PDI/F8BT	173.9 (±1.3)	±1.5		
PDI/PFB	164.3 (±2.0)	±2.2		
PDI/P3HT	199.0 (±15.2)	±6.5		

[a] Excitation was at $\lambda = 514$ nm, in the PL measurements, so as to preferentially photoexcite the pery-PIC component.

(F8BT) were supplied by Cambridge Display Technology Ltd., UK. The PFB was characterized as having molecular weights $m_p = 135$K and $m_n = 60$K, polydispersity = 2.8, and quantum-yield efficiency of 27%. The F8BT had $m_p = 147$K, $m_n = 97$K, polydispersity = 1.94, and quantum yield of 83%.

Bulk-heterojunction blend photovoltaic devices were fabricated for these experiments, using an indium−tin oxide (ITO) anode and a thermally evaporated aluminum cathode (Figure 5a, inset). The anode was preplanarized with a thin layer of PEDOT:PSS (poly(3,4-ethylenedioxythiophene):poly(styrenesulfonate) from Cambridge Display Technology Ltd.), which was baked in air at 150 °C for 30 min. The active layers of the devices were spin-coated from 12 mg/mL solutions of chloroform (HPLC anhydrous, Sigma Aldrich), and components were blended so as to give equal weight fractions; typical spinning parameters were 1000 rpm (acceleration ~50 rad/s^2) for 60 s at room temperature. The active layer thicknesses and roughness were determined using stylus profilometry and atomic force microscopy, respectively (see Table 1). The thermal evaporation of the Al cathode was performed under a vacuum of 1×10^{-6} mbar, at a deposition rate of ~1 nm/s, to a thickness of 100 nm. The devices were then "legged" to allow electrical connection and encapsulated in glass using an epoxy resin and hardener (Robnor Resins Ltd., UK), without the need for additional thermal annealing (Figure 5b, inset). Typical device-pixel areas after encapsulation were 1.5 × 4 mm.

The devices were tested at room temperature, under illumination from a calibrated thermal white-light source and monochromator, using a Keighley 195 DMM system parameter analyzer and a Keighley 237 source measure unit. The illumination source was focused down to a spot size of ~1 mm^2. Intensity dependence measurements were taken using the same electrical apparatus, but with illumination via a $\lambda = 525$ nm LED connected to a calibrated variable external power supply.

The tapping-mode atomic force micrographs described in this paper were taken with a Veeco Nanoscope IIIa instrument, operating under ambient non-cleanroom conditions, using software version 5.12 rev. B.

For photoinduced absorption spectroscopy, the film samples were placed under vacuum at room temperature and optically pumped with a modulated $\lambda = 488$ nm, continuous-wave Ar ion laser source, at an excitation density of ~0.1 W/cm^2, with the films having a measured optical density of ~1.0 at this wavelength. The sample is then probed for spectral features of photoinduced absorption, using a white-light source and lock-in amplifier.

Normal-incidence UV−vis absorption measurements were made using a Hewlett-Packard 8453 spectrophotometer. Photoluminescence (PL) measurements were taken using a $\lambda = 514$ nm Ar ion laser source of a few milliwatts intensity and a fiber-coupled CCD spectrometer; quantitative PL efficiency measurements were possible with the use of a calibrated integrating sphere.[12]

Ellipsometric measurements were made using a J.A. Woollam M-2000 diode-array rotating compensator ellipsometer with a xenon light source, over a wavelength range of 245−900 nm. Ellipsometry measures the change in polarization of light as a function of incident angle and wavelength for p (parallel) or s (senkrecht) polarized light after reflection or transmission by the sample, with the optical constants, n (refractive index) and k (extinction coefficient) being determined using an optical model in which the parameters are adjusted iteratively to give the best fit. Samples investigated in this work were modeled using J.A. Woollam Co. WVase32 software, which uses a Levenberg−Marquardt algorithm for fitting.

3. Results

Using previously reported protocols,[8,10,13] as also described in the Experimental Section, bulk-heterojunction blend devices were fabricated for these experiments, using an indium−tin

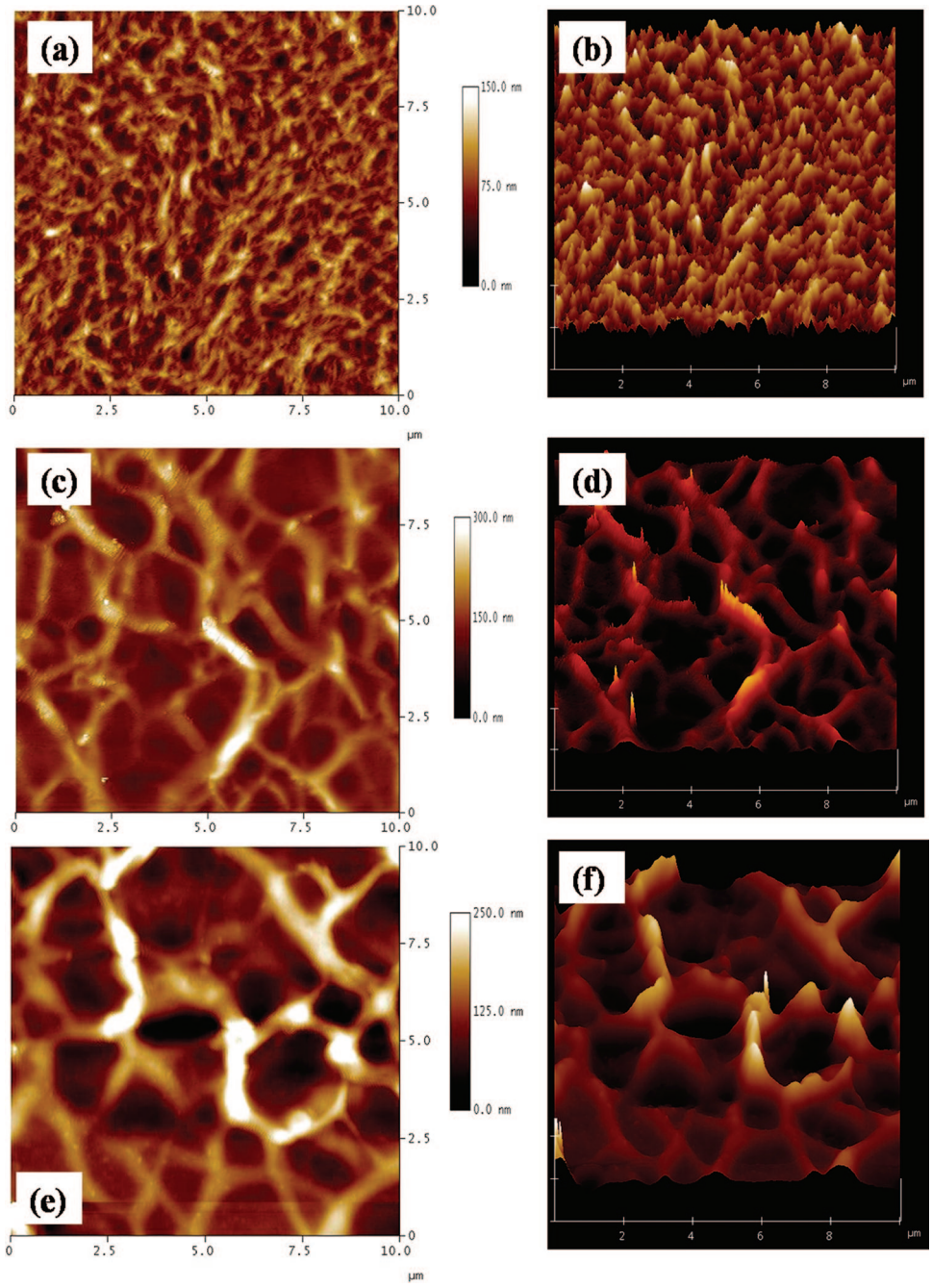

Figure 2. Tapping mode AFM images of ~1:1 weight ratio blends of pery-PIC with (a) P3HT, (c) PFB, and (e) F8BT, as spin-coated into thin films from chloroform solution. The length (in microns) and height scales are as indicated. Corresponding 3-dimensional projections, at a viewing angle of 30° from the substrate normal and with common height scales, are shown in (b), (d), and (f), respectively.

oxide (ITO) anode and a thermally evaporated aluminum cathode (Figure 3a, inset). A key strategy was to produce devices in which the optical cross section of the sensitizing component (pery-PIC vs PDI) was as closely matched as reasonably possible, based upon literature values of the extinction coefficients of PDI and the other conjugated polymer components.[14] More detailed measurements of the active-layer thicknesses, using a technique of stylus profilometry, are given in Table 1. Previous studies of PDI/conjugated-polymer PV devices[13] have shown these 1:1 weight ratios to give near-optimal performance, and while the device parameters are often seen to vary considerably as a function of active layer thickness, the measured values of thickness are also similar between the comparative pery-PIC and PDI blends to within experimental error and allowance for surface topography.

It can be seen from the atomic force microscopy (AFM) images in Figures 2 and 3 that the morphology of the pery-PIC and PDI blends are very different. The pery-PIC macromolecules tend to form large bundles, with phase separation on scales of 100s to 1000s of nanometers, which appear to lie in the plane of the film. The height of the bundles is of the same order as the film thickness (~100 nm), while their width is of the order of hundreds of nanometers. The mean roughnesses of these films, as measured by AFM, are given in Table 1. In contrast, the PDI analogue blends show smaller features of the order of tens of nanometers, with phase separation on a significantly smaller scale (Figure 3), and some evidence of perylene aggregation in the case of the PDI/P3HT blend. The presence of the polyisocyanide chain hence drastically alters the morphol-

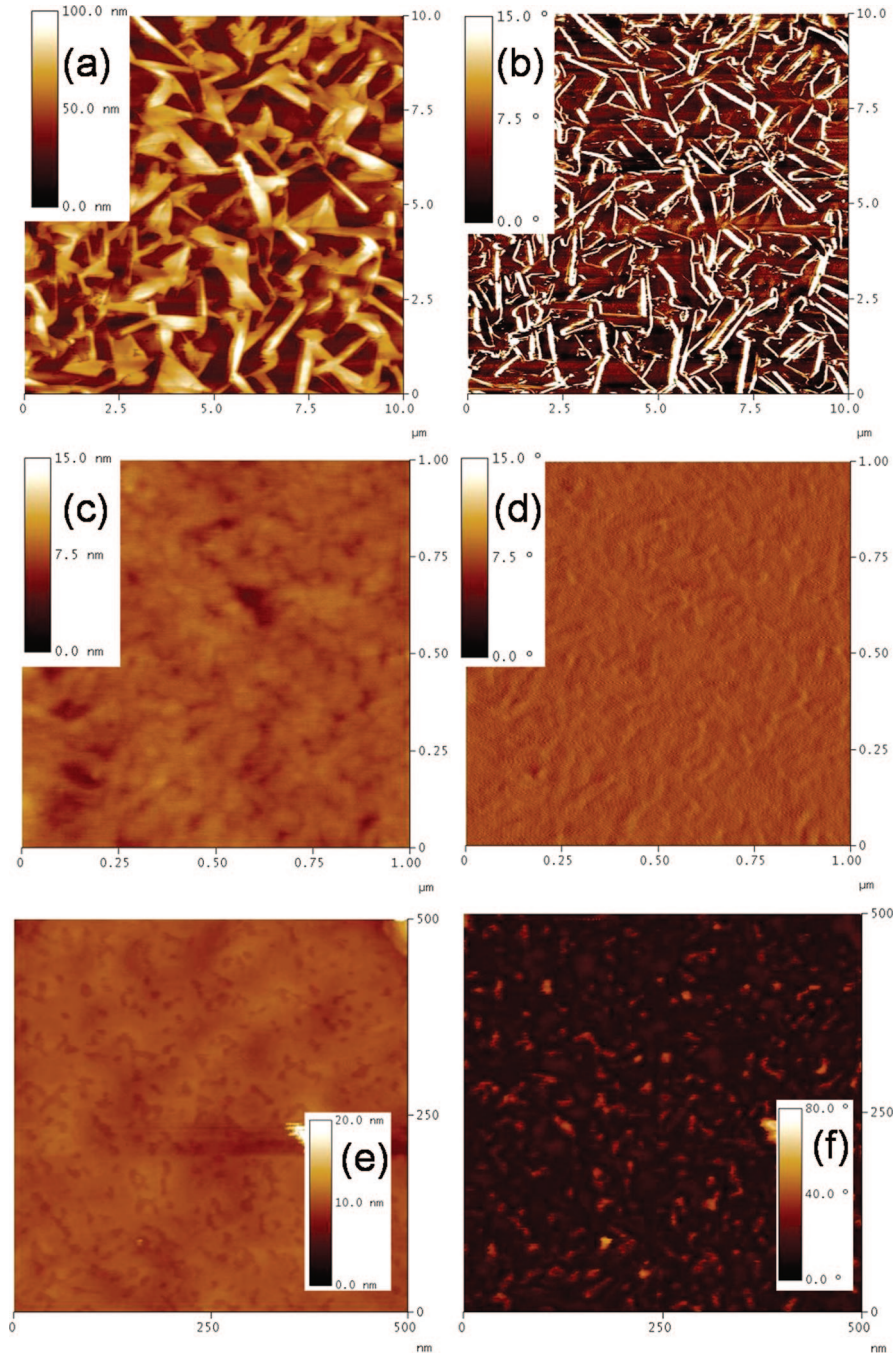

Figure 3. Tapping mode AFM images of ~1:1 weight ratio blends of PDI monomer with (a) P3HT, (c) PFB, and (e) F8BT, as spin-coated into thin films from chloroform. The length (in microns) and height scales are as indicated. Corresponding signal-phase plots are shown for clarity, in (b), (d), and (f), respectively.

ogy, on which the transport properties are expected to strongly depend.

Using such an approach, the effect on device performance due to variation in the material phase separation and entropy of mixing between the electron-donor material and the PIC can also be studied. There is also a significant difference in behavior between the pery-PIC blends with P3HT, PFB, and F8BT (Figure 2). The P3HT blend shows phase separation on length scales of ~100 nm, with some evidence of the pery-PIC forming smaller bundles, which are well dispersed within the P3HT phase, confirming earlier studies of this blend system.[15] By contrast, the F8BT blend shows a more complete phase separation on length scales of microns, with the pery-PIC forming more extended bundles, sometimes rising 100−200 nm out of the plane of the film, giving a mean film roughness in excess of ±30 nm. The pery-PIC/PFB blend appears to show characteristics which are intermediate between these two other cases.

The encapsulated devices were tested at room temperature, under illumination from a calibrated thermal white-light source and monochromator, using an $I-V$ parameter analyzer.[8,13] The external quantum efficiency (EQE) spectra of the PV devices are given in Figure 4. The EQEs of <4% are relatively low, as compared to state-of-the-art organic photovoltaics, but typical of many blend systems using perylene-based materials.[8,13,15,16] It can be seen that the peak EQE with pery-PIC is substantially higher than that with the PDI analogue in the P3HT (2.7% compared to 1.0%) and PFB (3.6% compared to 0.6%) blends, but smaller in the F8BT blends (0.6% compared to 1.3%).

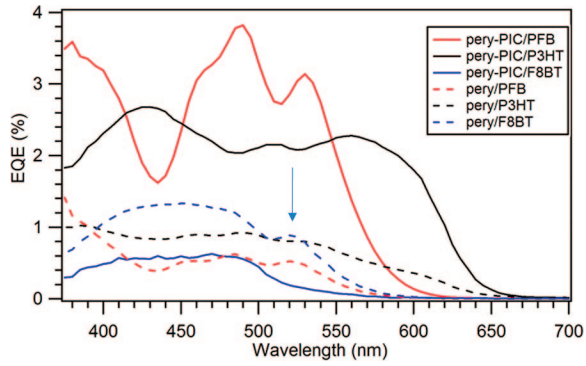

Figure 4. External quantum efficiency (EQE) vs wavelength of photovoltaic blends of pery-PIC with PFB (1:1.3 weight ratio), P3HT (1:1), and F8BT (1:1), as indicated. For comparison, the EQE spectra of analogous PDI blends are also shown (dashed lines). In the case of PDI/F8BT, the position of the long-wavelength feature, absent in the case of pery-PIC/F8BT, is indicated by an arrow.

Table 2. Representative Values for the Open-Circuit Voltage, Short-Circuit Current, Fill Factor, and Maximum Extracted Power for Each of the Pery-PIC and PDI Photovoltaic Blends Studied, As Indicated[a]

sample	V_{oc} (V)	I_{sc} (mA/cm^2)	fill factor	$I_{sc}V_{oc}$ (μW/cm^2)	P_{max} (nW/cm^2)	ε
PDI/P3HT	0.30	4.7×10^{-4}	0.21	0.141	29.6	
pery-PIC/P3HT	0.19	4.8×10^{-3}	0.41	0.912	373.9	12.6
PDI/PFB	0.07	4.5×10^{-4}	0.24	0.032	7.7	
pery-PIC/PFB	0.42	6.4×10^{-4}	0.31	0.269	83.4	10.8
PDI/F8BT	0.27	6.6×10^{-4}	0.26	0.178	46.3	
pery-PIC/F8BT	0.35	4.4×10^{-4}	0.30	0.154	46.2	1.0

[a] The relative enhancements (ε) of the power extraction efficiencies between analogous pery-PIC and PDI blends are also given. All devices were tested under illumination of intensity ~0.1 mW/cm^2 and at the wavelength of peak EQE performance. Device fill factors are defined as per usual convention. Note that numerical values are quoted here without errors for clarity. Variation between different pixels allows estimation of the errors in EQE (measured here as 0.0−4.0%) as <0.15%, in I_{sc} (measured here as 0−80 nA) as <2 nA, and in V_{oc} (measured here as 0.0−0.5V) as <0.02 V.

The data in Figure 5 show the $I-V$ characteristics under illumination for pery-PIC/P3HT and pery-PIC/PFB blends, together with the corresponding PDI devices. It is clear that there are significant enhancements in performance, in terms of both the device "fill factors" and the maximum extracted power. By comparison, the pery-PIC/F8BT devices show no such improvements from the PDI analogue case. A more general comparison of the performance of PV devices using the pery-PIC material, as compared to the analogous devices using PDI, is displayed in Table 2. Taking all the pertinent parameters into consideration, the enhancement factors in the power conversion efficiency are calculated to be 12.6 and 10.8 in the cases of P3HT and PFB, respectively, but there is little or no change for F8BT. While there are no simple patterns emerging across the different blend systems, the particularly large increase in short-circuit current (I_{sc}) in the case of P3HT suggests that the overall improvement in performance is due to an increased density of free charges, possibly due to the improved ordering of perylene units at the heterojunction interfaces.[17] By contrast, the large increase in open-circuit voltage (V_{oc}) in the case of PFB is rather indicative of improved efficiency of geminate charge separation and free-charge collection, possibly due to better connectivity and carrier conductance in the pery-PIC phase of the blend.

To further elucidate these issues, quantitative photoluminescence (PL) efficiency measurements were made on the samples; the relevant PL spectra are shown in Figure 6c and the quantitative data in Table 1. Thin films of the pery-PIC material were found to have a PL efficiency of 8.2%, and comparison of this value with those of the pery-PIC blends gives some indication of the degree to which luminescence is "quenched" due to charge separation. Quenching was found to be most prevalent in the pery-PIC/P3HT blend and weakest in the pery-PIC/F8BT blend; the lack of quenching in the latter case being qualitatively evident in the fluorescence microscope image of Figure 6d, which shows the intense PL from the F8BT phase of this blend as compared to the darker phase-separated pery-PIC bundles.

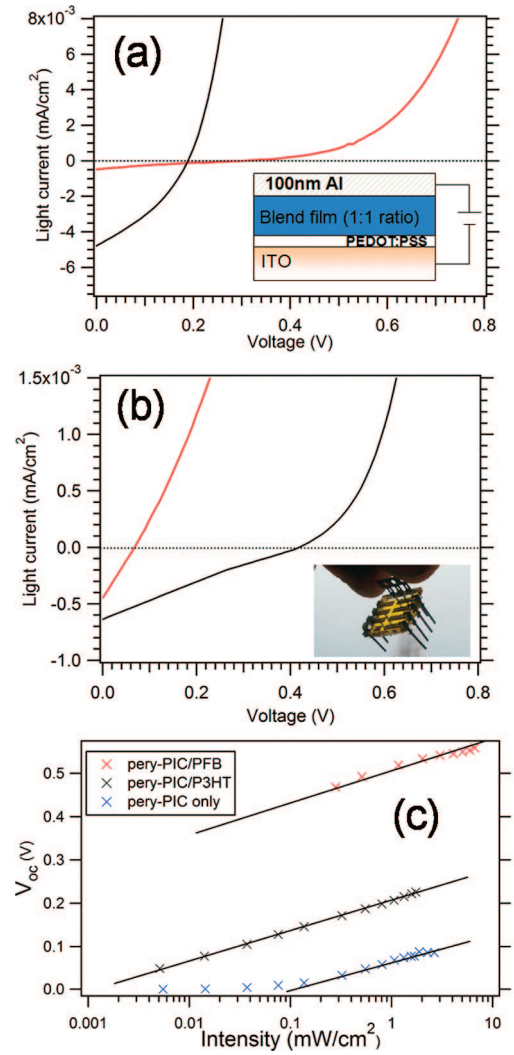

Figure 5. Current−voltage characteristics of photovoltaic devices, under conditions of peak EQE performance and illumintion intensity ~0.1 mW/cm^2. (a) 1:1 blend of pery-PIC with P3HT (black line), as compared to the analogous PDI/P3HT device (red). (b) 1:1 blend of pery-PIC with PFB (black), as compared to the analogous PDI/PFB device (red). A schematic of device structure and a photograph of a final encapsulated device are shown as insets. (c) Open-circuit voltages of pery-PIC/PFB and pery-PIC/P3HT photovoltaic devices, as a function of excitation intensity, measured at the wavelength of greatest EQE. The data obtained from a device containing only the pery-PIC material are shown for reference. The square-root power law dependence is clearly evident in these semilogarithmic plots (i.e., $V_{oc} \sim \alpha \log\{\text{intensity}\}$), with the extracted values of α all being in the range of 0.48−0.51.[18]

Finally, measuring V_{oc} for each of the device systems as a function of excitation intensity in the range of ~0.001−10 mW/cm^2 (see Figure 5c), a square-root power law dependence was observed in all cases, as might be expected when the principal loss mechanism in the device is bimolecular recombination.[18] Interestingly, devices incorporating 1:1 weight blends of pery-

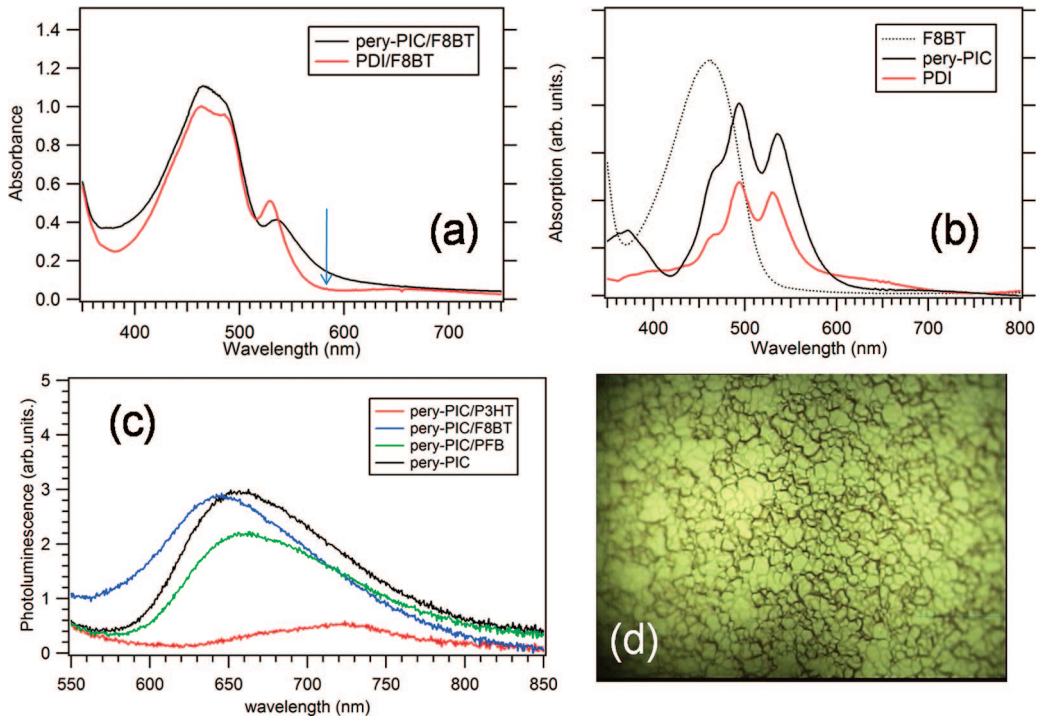

Figure 6. (a) Absorbance spectra for ~100 nm thick films of 1:1 weight ratio pery-PIC/F8BT and PDI/F8BT blends. The arrow indicates the point at which we observe reduced oscillator strength in the PDI/F8BT spectrum at around $\lambda = 590$ nm. For comparison, representative absorption spectra for thin films of F8BT, PDI, and pery-PIC are shown in (b). (c) Photoluminescence (PL) spectra of 1:1 weight ratio blends of thin-films of all pery-PIC blends studied, together with that of a thin film of the pery-PIC material only. Excitation was at $\lambda = 514$ nm, so as to preferentially photoexcite the pery-PIC component. (d) A fluorescence microscope image (magnification ×100, N.A. = 0.8) of the pery-PIC/F8BT blend, under UV/blue excitation. The approximate area of the image is 130 × 100 μm.

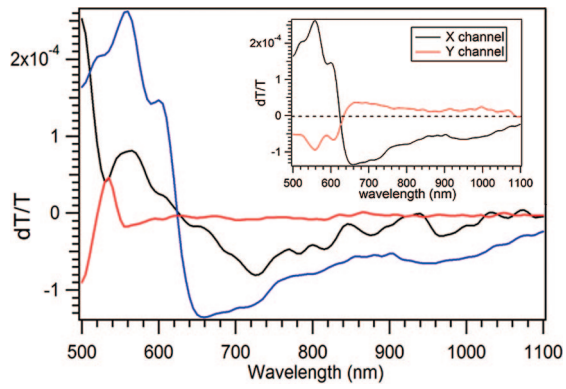

Figure 7. Room temperature photoinduced absorption (PIA) spectra, showing fractional change in transmission vs wavelength, for thin films of 1:1 weight ratio blends of pery-PIC with P3HT (blue), PFB (black), and F8BT (red). The inset shows the X channel (in phase) and Y channel (quadrature) PIA spectra for the pery-PIC/P3HT blend, when using a signal-modulation frequency of 225 Hz. Photoexcitation was at $\lambda = 488$ nm in all cases.

PIC in an inert polystyrene matrix were also shown to exhibit a small open-circuit voltage at higher excitation intensities; the exact nature of charge generation and separation in this system is under further investigation.[19,20]

4. Discussion: Poor Performance of Pery-PIC/F8BT Blend Devices

Our results are also interesting in the context of recent work on PDI-based PV devices,[13] where F8BT blends were observed to out-perform blends of other notionally p-type semiconducting polymers such as PFB. While the driving force for charge separation depends on many other issues as well as energetics, this was somewhat surprising, given the accepted values of electron affinity and ionization energy for these materials (2.3 eV/5.1 eV for PFB, 3.5 eV/5.9 eV for F8BT), as compared to that of PDI (3.8 eV/6.1 eV).[21,22]

In order to gain further insight into the photophysical differences between blends, photoinduced absorption spectroscopy (PIA) was performed on identical thin films to those used for devices (Figure 7). Quasi-steady-state PIA experiments were carried out under vacuum and at room temperature, following widely reported methods[23] (see Experimental Section). In the case of pery-PIC/P3HT, we see very strong signals of perylene anion species[24] between $\lambda = 650$ and 800 nm, reaffirming the general (perylene)$^-$/(p-type)$^+$ photovoltaic action of these blends. Similarly, for the pery-PIC/PFB there is a discernible photoinduced absorption feature at ~700 nm. No such features are seen, however, for the pery-PIC/F8BT blend in this wavelength range, indicating that either (a) the recombination of charges is very rapid, so that they cannot be seen by this steady state experiment, or (b) the densities of interfacial charge generation are very much lower. Hence, these direct measurements of the charged states in the blends are strongly consistent with the earlier discussion of PL quenching effects due to interfacial charge separation.

Further work is in progress to make detailed lifetime measurements of the ionized states observed in these PIA experiments, with the goal of better understanding the dynamics of charge separation and recombination in pery-PIC-based photovoltaic blends.

It should be noted that the pronounced long-wavelength shoulder at around 500−550 nm in the action spectrum of PDI/F8BT devices is absent in the case of pery-PIC/F8BT (see Figure 4). This long-wavelength feature however is present in the UV−vis absorption spectra of pery-PIC/F8BT and PDI/F8BT blends (Figure 6a). The same absorption feature has also been observed in blends of low PDI loadings (~0.3 wt %) in inert

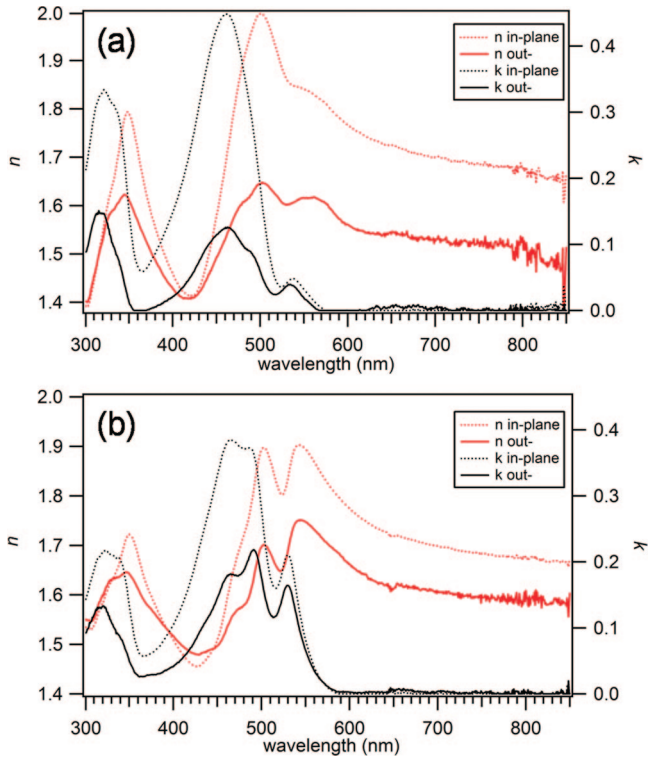

Figure 8. Thin-film ellipsometry studies using ~1:1 weight ratio blends of (a) pery-PIC/F8BT and (b) PDI/F8BT. The in-plane and out-of-plane optical constants ($N = n + ik$) are as indicated.

polystyrene.[13] Well-ordered perylene stacks (crystalline aggregates) in these particular PDI/F8BT blends can be ruled out, as there is no indication of their spectral signature at $\lambda = 590$ nm in the UV−vis absorption spectra,[13] nor is there any strong evidence of such aggregates in the AFM studies (Figure 3c). The observed increase in the spectral width of the absorption band around 500−550 nm in the pery-PIC/F8BT blend is commensurate with a slight increase in the oscillator strength of the 590 nm spectral region. It is suggested that the F8BT phase can efficiently solubilize the perylene (PDI) but not the pery-PIC component, which would also offer explanation of why the action spectra of the two systems are different in the spectral region of 500−550 nm. It is clear from the morphology of the pery-PIC blends (Figure 2) that the nanoscale domains observed in self-organized films of the free PDI monomer,[25,26] which might allow a solubilization of PDI in the more crystalline F8BT, are suppressed. Optimized packing of the pery-PIC aggregates and the relatively large length scales of phase separation (Figure 2e) allow excitons to localize and to deactivate within the pery-PIC moieties without reaching the interfaces with F8BT. As a result, this spectral region is not participating in the action spectra. Furthermore, these are interesting findings as they suggest that exciton trapping, but not carrier trapping, is the principal mechanism responsible for the low EQEs obtained from this system.

The fact that the arrangement of the perylene moieties around the PIC template is found to positively influence the performance of devices based on crystalline P3HT, but not the devices based on crystalline F8BT, suggests that apart from suppressing PDI aggregation there is also an issue regarding the orientation of the perylene moieties with respect to the plane of the device substrate. The AFM studies in Figures 2 and 3 do not allow a complete understanding of such orientational effects, and the lack of long-range crystallinity in the pery-PIC films would make X-ray diffraction studies difficult to attain and interpret. However, we were able to obtain ellipsometric studies[27] of the pery-PIC/F8BT and PDI/F8BT blends (see Figure 8). The optical constants (refractive index n and extinction coefficient k) could be fitted continuously and consistently as a function of wavelength for these particular thin films.

For the pery-PIC/F8BT blend, there are differences between the in-plane and out-of-plane results, with the k component due to the low-energy pery-PIC absorption peak being substantially blue-shifted in the out-of-plane case ($\lambda = 532$ nm, as compared to $\lambda = 538$ nm in-plane). This would be consistent with the PIC chain lying predominantly in an in-plane orientation relative to the substrate, with the red shift in absorption due to exciton delocalization along chains[5,7] being most prevalent in the in-plane direction. In the PDI/F8BT control film, there is no such effect. The long wavelength (transparent) in-plane/out-of-plane birefringence is also very much smaller (<0.1) for the PDI/F8BT blend relative to the pery-PIC/F8BT (~0.2). Commensurately, the birefringence at the F8BT absorption peak is also reduced from 0.36 to ~0.20; there are similar changes in the dichroism of the k components.

We propose that the physical interpretation of this is that the rigid F8BT segments have a greater tendency to lie in plane in the pery-PIC blend, possibly due to the much greater degree of phase separation, as evidenced in Figure 2. This could be another underlying reason for the poor efficiency of photoinduced charge transfer process; as the pery-PIC tends to lie in plane, the perylene groups will tend to be orientated in an orthogonal direction to the in-plane F8BT dipoles.[28]

5. Conclusions

In conclusion, photovoltaic blend devices incorporating perylene-substituted polyisocyanide materials have been demonstrated to show an order of magnitude improvement in power conversion efficiency, as compared to analogous blend architectures using a perylene (PDI) monomer. Given the ubiquitous nature of the chemical synthesis techniques involved, we anticipate that the use of polyisocyanide chains as a molecular template may soon be extended to state-of-the-art photovoltaic materials, such as the polythiophene/fullerene systems.[29] The fact that pery-PIC moiety is found to positively influence the performance of devices based on crystalline P3HT but not the devices based on crystalline F8BT suggests that optimal orientation of the perylene moieties with respect to the plane of the device substrate is also an important factor. Bearing this in mind, future work will also involve the use of techniques aimed at achieving ordering of substituted polyisocyanide strands on the mesoscale, in order to give optimized geometries for charge collection in PV devices. This might include the use of suitable attachment chemistry to grow rigid "brushes"[30,31] of the material out of the plane of one or both electrodes.

Acknowledgment. This work was supported by the ESF-SONS2; SUPRAMATES project. P.E.K. acknowledges EPSRC (UK) for funding through the Next Generation Electrophotonics program Grant EP/C540336. C.E.F. thanks the Leverhulme Trust (UK) for an Early Career Fellowship. The authors thank Dr. K. R. Kirov and H. Clubb of the Cavendish Laboratory for help and advice with the experimental work described in this paper and also A. Abrusci for providing the photographic images displayed.

References and Notes

(1) Cornelissen, J. J. L. M.; Donners, J. J. J. M.; de Gelder, R.; Graswinckel, W. S.; Metselaar, G. A.; Rowan, A. E.; Sommerdijk, N. A. J. M.; Nolte, R. J. M. *Science* **2001**, *293*, 676.
(2) Schwartz, E.; Kitto, H. J.; de Gelder, R.; Nolte, R. J. M.; Rowan, A. E.; Cornelissen, J. J. L. M. *J. Mater. Chem.* **2007**, *17*, 1876.

(3) Kitto, H. J.; Schwartz, E.; Nijemeisland, M.; Koepf, M.; Cornelissen, J. J. L. M.; Rowan, A. E.; Nolte, R. J. M. *J. Mater. Chem.* **2008**, *18*, 5615.
(4) Blankenship, R. E. *Molecular Mechanisms of Photosynthesis*; Blackwell: Oxford, UK, 2001.
(5) Hernando, J.; de Witte, P. A. J.; van Dijk, E. M. H. P.; Korterik, J.; Nolte, R. J. M.; Rowan, A. E.; Garcia-Paraj, M. F.; van Hulst, N. F.*Angew. Chem., Int. Ed.* **2004**, *43*, 4045.
(6) de Witte, P. A. J.; Hernando, J.; Neuteboom, E. E.; van Dijk, E. M. H. P.; Meskers, S. C. J.; Janssen, R. A. J.; van Hulst, N. F.; Nolte, R. J. M.; Garcia-Parajo, M. F.; Rowan, A. E. *J. Phys. Chem. B* **2006**, *110*, 7803.
(7) Schwartz, E.; Palermo, V.; Finlayson, C. E.; Huang, Y.-S.; Otten, M. B. J.; Liscio, A.; Trapani, S.; González-Valls, I.; Brocorens, P.; Cornelissen, J. J. L. M.; Peneva, K.; Müllen, K.; Spano, F.; Yartsev, A.; Westenhoff, S.; Friend, R. H.; Beljonne, D.; Nolte, R. J. M.; Samori, P.; Rowan, A. E. *Chem.—Eur. J.* **2009**, in press.
(8) Dittmer, J. J.; Marseglia, E. A.; Friend, R. H. *Adv. Mater.* **2000**, *12*, 1270.
(9) Finlayson, C. E.; Friend, R. H.; Otten, M. B. J.; Schwartz, E.; Cornelissen, J. J. L. M.; Nolte, R. J. M.; Rowan, A. E.; Samorı´, P.; Palermo, V.; Liscio, A.; Peneva, K.; Müllen, K.; Trapani, S.; Beljonne, D. *Adv. Funct. Mater.* **2008**, *18*, 3947.
(10) Hoppe, H.; Sariciftci, N. S. *J. Mater. Res.* **2004**, *19*, 1924.
(11) Weight ratio blends must also take into account the fraction of the total molecular mass of pery-PIC which is accounted for by the active perylene component; the structural formula shown in Figure 1a implies that this fraction is 79.8%.
(12) Greenham, N. C.; Samuel, I. D. W.; Hayes, G. R.; Phillips, R. T.; Kessener, Y. A. R. R.; Moratti, S. C.; Holmes, A. B.; Friend, R. H. *Chem. Phys. Lett.* **1995**, *241*, 89.
(13) Keivanidis, P. E.; Howard, I. A.; Friend, R. H. *Adv. Funct. Mater.* **2008**, *18*, 3189.
(14) Shikler, R.; Friend, R. H. *J. Appl. Phys.* **2007**, *102*, 013105.
(15) Palermo, V.; Otten, M. B. J.; Liscio, A.; Schwartz, E.; de Witte, P. A. J.; Castriciano, M. A.; Wienk, M. M.; Nolde, F.; De Luca, G.; Cornelissen, J. J. L. M.; Janssen, R. A. J.; Müllen, K.; Rowan, A. E.; Nolte, R. J. M.; Samori, P. *J. Am. Chem. Soc.* **2008**, *130*, 14605.
(16) Granstrom, M.; Petritsch, K.; Arias, A. C.; Lux, A.; Andersson, M. A.; Friend, R. H. *Nature (London)* **1999**, *395*, 257.
(17) Veldman, D.; Ipek, O.; Meskers, S. C. J.; Sweelssen, J.; Koetse, M. M.; Veenstra, S. C.; Kroon, J. M.; Bavel, S. S.; Loos, J.; Janssen, R. A. J. *J. Am. Chem. Soc.* **2008**, *130*, 7221.
(18) Ramsdale, C. M.; Barker, J. A.; Arias, A. C.; MacKenzie, J. D.; Friend, R. H.; Greenham, N. C. *J. Appl. Phys.* **2002**, *92*, 4266.
(19) Huang, Y.-S. Sequential Energy and Electron Transfer in Polyisocyanopeptide based Multichromophoric Arrays. Ph.D. Thesis, University of Cambridge, U.K., **2008**; Chapter 6.
(20) Zhang, G.; Thomas, J. K. *J. Phys. Chem. A* **1998**, *102*, 5465.
(21) Ulgut, B., private communication, **2008**.
(22) Erten, S.; Meghdadi, F.; Gunes, S.; Koeppe, R.; Sariciftci, N. S.; Icli, S. *Eur. Phys. J. Appl. Phys.* **2007**, *36*, 225.
(23) Dhoot, A. S.; Greenham, N. C. *Adv. Mater.* **2002**, *14*, 1834.
(24) Holman, M. W.; Yan, P.; Adams, D. M.; Westenhoff, S.; Silva, C. *J. Phys. Chem. A* **2005**, *109*, 8548.
(25) Graaf, H.; Unold, T.; Mattheus, C.; Schlettwein, D. *J. Phys. D: Appl. Phys.* **2008**, *41*, 105112.
(26) Rybak, A.; Pisula, W.; Jung, J.; Ulanski, J. *Thin Solid Films* **2008**, *516*, 4201.
(27) Ramsdale, C. M.; Greenham, N. C. *J. Phys. D: Appl. Phys.* **2003**, *36*, L29–L34.
(28) Alloway, D. M.; Armstrong, N. R. *Appl. Phys. A: Mater. Sci. Process.* **2009**, in press.
(29) Ma, W.; Yang, C.; Gong, X.; Lee, K.; Heeger, A. J. *Adv. Funct. Mater.* **2005**, *15*, 1617.
(30) Snaith, H. J.; Whiting, G. L.; Sun, B.; Greenham, N. C.; Huck, W. T. S.; Friend, R. H. *Nano Lett.* **2005**, *5*, 1653.
(31) Lim, E.; Tu, G.; Schwartz, E.; Cornelissen, J. J. L. M.; Rowan, A. E.; Nolte, R. J. M.; Huck, W. T. S. *Macromolecules* **2008**, *41*, 1945.

MA801959W